Nanoscale

Accepted Manuscript

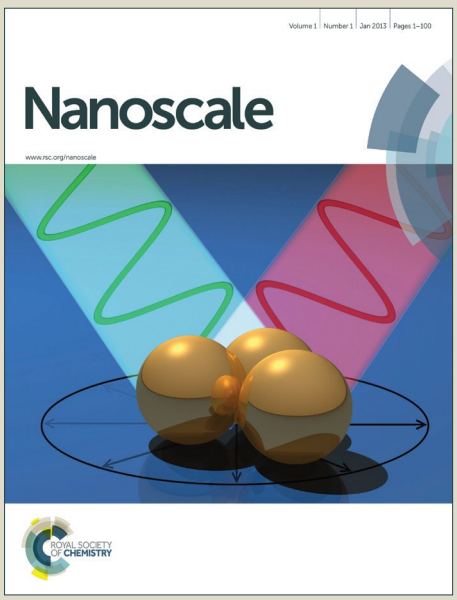

ROYAL SOCIETY OF CHEMISTRY

www.rsc.org/nanoscale

Nanoscale

RSCPublishing

ARTICLE

Role of hydrogen in chemical vapor deposition growth of MoS_2 atomic layers

Cite this: DOI: 10.1039/xoxxoooooox

Xiao Li,[a,b] Xinming Li,[c] Xiaobei Zang,[a] Miao Zhu,[a,b] Yijia He,[a,b] Kunlin Wang,[a] Dan Xie,[d] Hongwei Zhu,[*a,b]

Received ooth January 2015,
Accepted ooth January 2015

DOI: 10.1039/xoxxoooooox

www.rsc.org/

Hydrogen plays a crucial role in graphene chemical vapor deposition (CVD) growth. Here, we have revealed the role of hydrogen in a two-step MoS_2 CVD growth. Our study demonstrates the following: i) as an inhibitor of thermal-induced etching effect in the process of continuous films growth; ii) as a promoter of desulfurization reaction by decreasing S/Mo atomic ratio and oxidation reaction of the obtained MoS_x ($0<x<2$) films. High hydrogen content of more than 100% in argon would form nano-sized circle-like defects and damage the continuity and uniformity of the film. Continuous MoS_2 films with high crystallinity and nearly perfect S/Mo atom ratio were finally obtained after sulfurization annealing at hydrogen content in the range of 20%~80%. This insightful understanding reveals a crucial role of hydrogen in MoS_2 CVD growth and paves a way for the controllable synthesis of two-dimensional materials.

Introduction

Many breakthroughs have been achieved on both fundamental and applied research of graphene.[1-3] In recent years, graphene-like two-dimensional (2D) materials of transition metal dichalcogenides (TMDCs) have attracted increasingly research interests.[4-5] Molybdenum disulfide (MoS_2), as a typical TMDC with a particular direct band gap of 1.8 eV in monolayer and layer number dependence of band structure, has been exhibiting its biggest ambition to tackle the gapless problems of graphene.[6-7] Mechanical exfoliation is widely used in fundamental research because of the possibility of fabricating high quality 2D materials.[1,8] Nevertheless, this method might not be suitable for practical applications because of its low yield and failing to control sheet size and the number of layers. Hence, high-throughput preparation method for large-area 2D materials with desired dimensions is necessary to be developed for wafer-scale applications, such as integrated circuit fabrication.

Chemical vapor deposition (CVD) method is one of the most practical methods to prepare 2D materials, including graphene,[9] boron nitride (BN),[10] and MoS_2-like TMDCs.[11-15] The operation parameters of the method, such as growth atmosphere, partial pressure, reaction temperature, and duration, are critical for the quality of final obtained materials. In the CVD process, hydrogen (H_2) is believed to be a significant factor in regulating the growth atmosphere and the role of H_2 during the synthesis of graphene has been systematically studied in different points of view.[16-21] For examples, I. Vlassiouk and his coworkers[16] proposed that the growth of graphene domains was strongly dependent on the H_2 concentration in a mixed gas of argon (Ar) and a small amount of H_2. The role of H_2 in the process was not only as a catalyst promoting monolayer film growth, but as an etching reagent to significantly control the size and morphology of the graphene domains. M. Losurdo *et al*.[17] reported a real-time investigation on the CVD kinetic study by using methane (CH_4) and H_2 precursors on both polycrystalline copper (Cu) and nickel (Ni) substrates and revealed the behavior of competitive dissociative chemisorption of H_2 and the working mechanism of dehydrogenating chemisorption of CH_4. X. F. Zhang's group[18] made an attempt to replace the mixture of Ar and H_2 with high concentration H_2 or even pure H_2 as a buffer gas and found that the growth of graphene structures with unique edge morphologies was advanced. Intriguingly, B. Wu *et al.*[19] highlighted the ordered pattern formation of graphene flakes on liquid Cu surface in the preparation of single-layer and single-crystalline graphene flakes in highly regular and hexagonal symmetric shapes.

The study of preparing controllable CVD growth TMDCs-family 2D materials could be traced back to 2012. L. J. Li's group[11] first reported monolayer MoS_2 films formed on silicon dioxide (SiO_2) substrate in ambient environment by an approach through the sulfurization of Mo based compound, such as molybdenum trioxide (MoO_3). They then proposed another effective method to facilitate the synthesis of MoS_2

films in wafer scale.[12] Bi- or trilayer continuous MoS_2 films were obtained by simple thermal decomposition of pre-dip coated ammonium thiomolybdates ($(NH_4)_2MoS_4$) films. The electrical performance of this film was similar with that of the materials fabricated by mechanical exfoliation. Later, many groups developed various CVD techniques to achieve TMDCs films.[13,15] However, few researches have focused on the effect of growth atmosphere during the domain formation. Y. Zhang *et al*.[21] demonstrated that the shape of monolayer WS_2 flakes could be managed from jagged to straight edge triangles by adding H_2 to the Ar gas flow. Furthermore, some joining triangle-shape WS_2 flakes were captured as abnormal structures. Based on the previous studies on H_2 critical function on graphene growth, it is reasonable to present that H_2 might have a similar effect on the growth of TMDCs films. Hence, more studies on the role of H_2 on the high-quality TMDCs film formation by CVD are necessary.

In this work, the contribution of H_2 to MoS_2 film preparation by CVD method was systematically studied. As illustrated in Scheme 1, thermolysis of $(NH_4)_2MoS_4$ films in subsequent annealing in sulfur (S) atmosphere were used to prepare few-layer continuous MoS_2 films on SiO_2 substrate based on previous procedure.[12] It was found that, with a low H_2 content in Ar (<10%), the thermal thinning effect was dominant, causing a discontinuous or even severely damage of MoS_x ($0<x<2$) film. If the H_2 content was increased to 20% or more, a striking phenomenon was observed. The intensity of the characteristic Raman peak of MoS_x was gradually decreased with decreasing S/Mo atomic ratio. It indicated that the film was gradually oxidized. Thus, H_2 with moderate content, which was 20%~40% in the first step of annealing, could inhibit thermal-induced oxidation reaction. As the H_2 content was increased to 100% or above, the obtained MoS_x films exhibited nano-sized circle-like defects, which may be caused by H_2-promoted desulfurization and chemical etching effect. Obviously, H_2 played a dual role in the process and excess H_2 might chemically react with unstable surface S sites, leading to the deterioration of films quality. In the second step sulfurization annealing, the active S atoms would energetically adsorb on remained molybdenum (Mo) sites in S atmosphere. After this step, as-prepared MoS_2 films possessed high crystallizing degree with nearly perfect S/Mo atomic ratio.

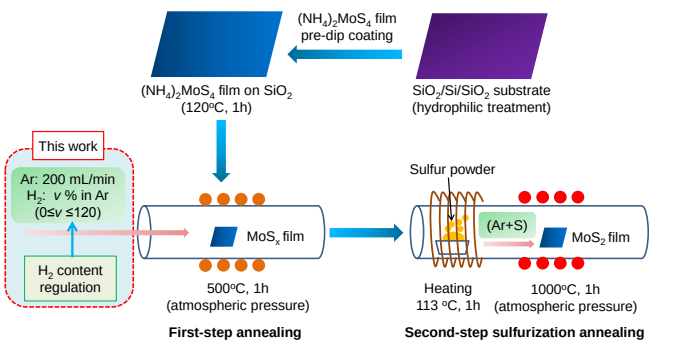

Scheme 1. Schematic illustration for the CVD growth of large-area MoS_2 film. This work studied the role of hydrogen during the first-step annealing.

Experimental

$SiO_2/Si/SiO_2$ substrate pre-treatment

300 nm SiO_2 on both sides of Si substrates were successively cleaned in acetone, absolute ethanol and deionized (DI) water, and each step was followed by an entire rinse with the subsequent solution. Next, the substrates were submersed in a mixture solution (NH_4OH: H_2O_2: DI water = 1:1:5) for hydrophilic treatment (30 min). $(NH_4)_2MoS_4$ precursor solution was prepared by dissolution $(NH_4)_2MoS_4$ (Alfa Aesar, 99.99%; 1 g) into 80 mL n-methylpyrollidone (NMP). The solution was sonicated for 2 h. At 80 °C, the precursor $(NH_4)_2MoS_4$ films were dip-coated onto SiO_2 at the speed of 650 μm/s. Next, the substrates were baked on a hot plate at 120 °C for 1 h.

MoS_x and MoS_2 films preparation

$SiO_2/Si/SiO_2$ substrates with uniform $(NH_4)_2MoS_4$ films were then moved into the center of a CVD furnace (Lindberg/Blue M). After exhausting process with Ar, the furnace was heated to 500 °C in 30 min under the protection of Ar/H_2. Ar flow rate was set as 200 mL/min, while the H_2 content was carefully controlled from 0% to 120% in Ar. The substrates were kept under 500 °C for 1 h and then quickly cooled down to obtain as-prepared MoS_x films (S/Mo atomic ratio $0<x<2$). To complete MoS_2 films preparation, a second-step sulfurization annealing in (Ar+S) was conducted in 1000 °C for 1 h. Sulfur powder was placed outside the hot zone and its vapor was introduced by mildly sublimating at ~113 °C. MoS_x films were turned into MoS_2 films with S/Mo atomic ratio of ~2.

Characterizations

Optical microscopy (ZEISS, Axio Scope A1; ProgRes CapturePro 2.7), Raman and PL spectroscopy (LabRAM HR Evolution, laser excitation 514.5 nm, 50 mW), XPS measurement (PHI Quantera SXMTM, Scanning X-ray MicroprobeTM), TEM (JEM-2010, 120-200 kV), AFM (Agilent 5100).

Results and discussion

A mixture gas of H_2 and Ar was used in the thermolysis process of pre-dip coated $(NH_4)_2MoS_4$ films on SiO_2 to form MoS_2 films. The content of H_2 was defined as volume concentration in Ar ($0\le v\le 120$), denoted as v%. The previous method,[12] in which the flow rate of $Ar:H_2$ was set as 4:1 at 1 Torr in the first annealing process of 500 ℃ to obtain MoS_2 thin films, was used in this work in the thermolysis of $(NH_4)_2MoS_4$ films under atmospheric pressure. The E^1_{2g} and A_{1g} modes in Raman spectra of MoS_2 films are considered as indicators of in-plane and out-of-plane vibration modes of S atoms, respectively.[22] When the content of H_2 was 0%, discrete MoS_x flakes were observed in the optical microscopy (OM) images (Fig. 1). No typical peaks (E^1_{2g} and A_{1g}) were found (Fig. S1), indicating that MoS_2 with crystal structure was not formed. If the H_2 content was increased to 5%, the MoS_x was more continuous in

some range even though no Raman peaks were seen yet (Fig. S1).

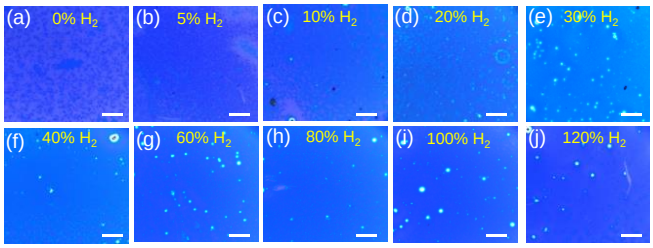

Figure 1. OM images of samples obtained with different H_2 concentrations (in Ar) after first-step annealing. (a) 0%. (b) 5%. (c) 10%. (d) 20%. (e) 30%. (f) 40%. (g) 60%. (h) 80%. (i) 100%. (j) 120%. Scale bars: 10 μm.

Several research groups reported that mechanically exfoliated MoS_2 flakes could be thinned down to monolayer by simply thermal annealing, whether in air[23] or under Ar protection.[24] Y. Huang *et al.*[25] developed this top-down synthesis method in the preparation of other 2D materials and proposed a self-stopping evaporative thinning method, in which the resultant MoS_x seemed to undergo a thermal sublimation process at extremely low H_2 content, leading to thinning or even damage of the films. The results revealed that H_2 was indispensable for the formation of continuous MoS_x films. If the H_2 content was increased to 10% or higher, continuous MoS_x films would be formed in large area, as shown in Fig. 1 and Fig. S2. Thus-synthesized films (5%~80% H_2) were multilayers, as shown in Fig. 2a-h, and their crystallinity was relatively poor, as indicated by the selected area electron diffraction (SAED) patterns.

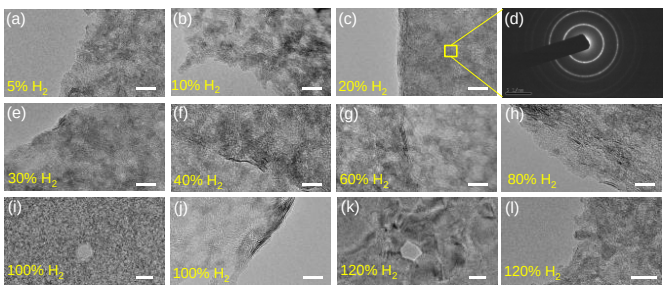

Figure 2. TEM characterizations of samples obtained with different H_2 concentrations (in Ar) after the first-step annealing. (a) 5%. (b) 10%. (c) 20%. (d) Corresponding SAED pattern of the marked area in (c). (e) 30%. (f) 40%. (g) 60%. (h) 80%. (i,j) 100%. (k,l) 120%. Scale bars: 10 nm in (a-c), (e-h), (j) and (l); 50 nm in (i) and (k).

Normalized Raman spectra of the samples with increasing H_2 content (10% to 120%) were shown in Fig. 3a. The intensity ratios between E^1_{2g}, A_{1g} of MoS_x and Si were closely related to the H_2 content.[13,22] As shown in the fitting tendency in Fig. 3b, the ratios of E^1_{2g}/Si and A_{1g}/Si reached maxima at H_2 content of ~20%. If H_2 content was below 20%, the thermal-induced etching effect would be still dominant, corresponding to the reduction in intensity of these two characteristic Raman peaks. If H_2 content was more than the critical value of 20%, the intensities of E^1_{2g} and A_{1g} were obviously decreased and even disappeared at 120% H_2.

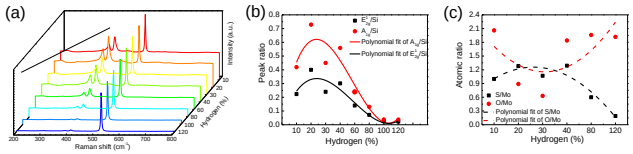

Figure 3. (a) Normalized Raman spectra with different H_2 concentrations. (b) Intensity ratio analysis for two typical Raman peaks (E^1_{2g} and A_{1g}) relative to Si peak calculated according to (a). (c) S/Mo and O/Mo atomic ratios as a function of H_2 concentration.

Raman spectra of the samples with H_2 content over 40% showed a linear downward trend, therefore the relatively large step-interval was enough for mechanism analysis. X-ray photoelectron spectroscopy (XPS) was used to understand the underlying mechanism. The H_2 contents of 10%, 20%, 30%, 40%, 80%, and 120% were chosen in the analysis. The evolution of the binding energy of Mo and S in the MoS_2 films was shown in Fig. 4. Both elemental bonding information and composition of Mo and S were obtained from XPS spectra. The peaks at ~229.5 and 232.7 eV were assigned to the Mo $3d_{5/2}$ and $3d_{3/2}$, respectively, of the core levels of Mo^{4+}. The peaks at 162.4 and 163.5 eV were attributed to the S $2p_{3/2}$ and $2p_{1/2}$, respectively, of divalent sulfide ions (S^{2-}). The intensity of the peak at ~235.9 eV, which was attributed to the $3d_{3/2}$ binding energy of Mo^{6+} and used to indicate the oxidation level of Mo resulting from the formation MoO_3[26] (as shown in the red square in Fig. 4), was obviously changed with H_2 content. It can be seen that the intensity was decreased to a minimum value with increasing H_2 content from 10% to 20%, indicating that H_2 was indispensable for MoS_x film formation, in agreement with the Raman result. The intensity of Mo^{6+} $3d_{3/2}$ peak was then gradually increased with increasing H_2 content, suggesting serious oxidation of as-prepared films. Hence, moderate H_2 content could inhibit the thermal-induced etching effect, in favour of the formation of continuous films in large area. However, the film would be re-oxidized gradually at H_2 content over 20%. At the H_2 contents of 80% and 120%, as shown in Fig. 4e,f, complicated peaks of Mo were observed in the range of 227 ~ 235 eV besides the Mo^{6+} $3d_{3/2}$ peak at 236 eV. It indicated that other Mo oxidation states of MoO_s ($0 \le s \le 3$) were formed as well. As analyzed in Fig. 4f, the sulfur was also oxidized at high H_2 contents. Because of the thermal effect at low H_2 content (<20%) and the oxidation effect at high H_2 content (>20%), the flow rate of H_2 should be carefully controlled in the formation process of MoS_x films in CVD. The stoichiometric ratios of S/Mo and O/Mo obtained from XPS were fitted and plotted in Fig. 3c. Despite the inevitable fluctuation in XPS data due to the inherent uneven distribution of samples prepared by CVD, the variation trends of the atomic ratios of S/Mo and O/Mo were clearly opposite, *i.e.*, the S/Mo ratio was increased first and then decreased, while the O/Mo ratio was decreased first and then increased. The maximum S/Mo ratio and the minimum O/Mo ratio were found at 20%

and 40% H_2 content, respectively. It indicated that the films with best quality could be formed at the H_2 content of 20%~40%, with relatively higher Raman peak intensity, lower oxidation degree, and excellent S/Mo atomic ratio.

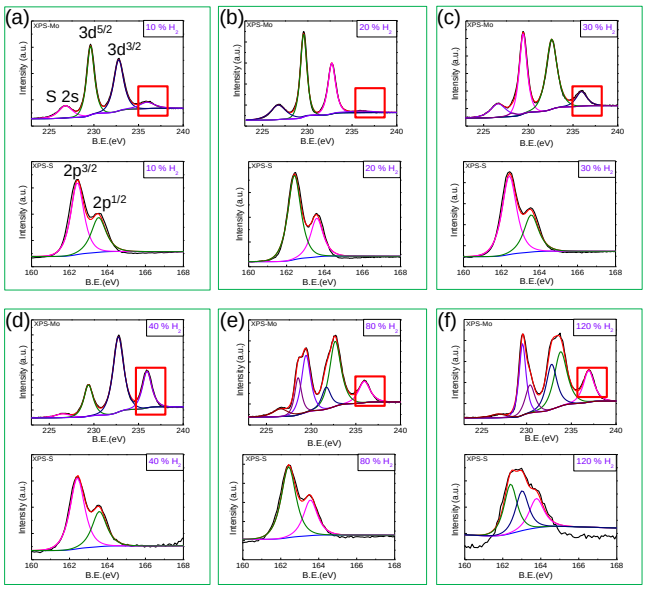

Figure 4. XPS spectra of Mo and S in MoS_2 films obtained with different H_2 concentration (in Ar) after first-step annealing. (a) 10%. (b) 20%. (c) 30%. (d) 40%. (e) 80%. (f) 120%.

During the formation process of continuous films on the SiO_2 substrate, H_2 mainly played two roles: thermal-induced etching and oxidation effect. It would also act as a promoter to cause aggravated re-oxidation. A working mechanism schematic of H_2 was illustrated in Fig. 5. When H_2 content was below 10%, the thermal-induced etching effect was predominant, leading to discontinuous and even damaged films. With increasing H_2 content (20%~80%), the energetically active H atoms were chemisorbed on the unstable S sites, breaking the relatively weak Mo-S bonds at high temperature. New chemical combination between H and S was formed (H_yS or HS_x, $0<y\leq2$, $0<x<2$). The desulfurization and synchronous oxidation reactions were illustrated in the following Formulas.[12,27] When H_2 content further increased to over 100%, the desulfurization process became more severe, resulting in the formation of circle-like defects.

$$(NH_4)_2MoS_4 + H_2 \xrightarrow{425\ ^\circ C} 2NH_3 + 2H_2S + MoS_2\ ^{[12,27]} \quad (1)$$

$$n(MoS_2) + \frac{(2-x)y}{2}H_2 \rightarrow n(MoS_x) + (2-x)H_yS\ (0<x<2; 0<y\leq2) \quad (2)$$

$$n(MoS_x) + nx(O^-) + \frac{n}{2}H_2 \rightarrow n(MoO_x) + nHS_x\ (0<x<2) \quad (3)$$

To further verify the hydrogen-promoting desulfurization mechanism, a second-step sulfurization annealing in Ar and S atmosphere was conducted. The samples obtained at 40% and 80% H_2 contents with S/Mo atomic ratios of 1.29 and 0.6, respectively, were used for sulfurization annealing. Transmission electron microscopy (TEM) characterizations were shown in Fig. 6a-f. Different from Fig. 2d, the SAED patterns showed dotted-ring feature, indicating that the crystallization degree was improved after annealing in sulfur atmosphere. The absence of Mo^{6+} $3d_{3/2}$ peak at ~235.9 eV indicated that Mo oxidation state was completely eliminated (Fig. 6g, h). The stoichiometric ratio of S/Mo measured by XPS was presented in Table 1. The ratio was very close to that of MoS_2 film. The thickness of as-prepared MoS_2 films was measured by Atomic Force Microscope (AFM), as shown in Fig. S3. Two typical Raman peaks were observed (Fig. 6i): E^1_{2g} at 385.337 cm^{-1} and A_{1g} at 406.283 cm^{-1} before sulfurization, and E^1_{2g} at 385.337 cm^{-1} and A_{1g} at 410.086 cm^{-1} after sulfurization. The peak spacing between E^1_{2g} and A_{1g} was increased from 21 to 25 cm^{-1} after the sulfurization process, as shown in Fig. S4b.

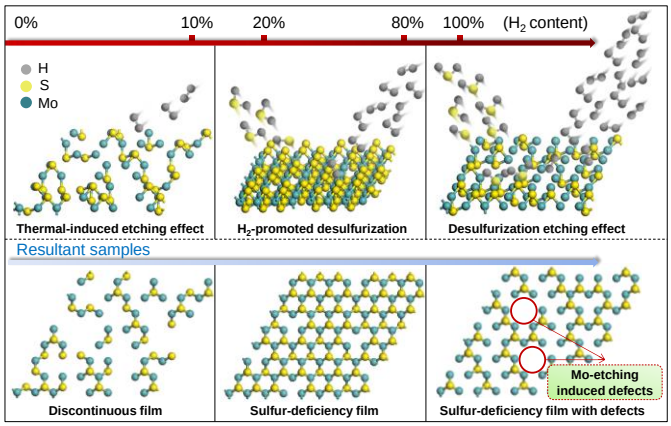

Figure 5. Schematic illustration of the working mechanism of H_2 in CVD of MoS_x film.

Raman mapping of samples treated at 40% H_2, 80% H_2, 40% H_2 (annealed), and 80% H_2 (annealed) was conducted to justify their uniformity, as shown in Fig. S5, ESI. The testing areas of 40×40 μm^2 for all samples were shown in Fig. S5a-d. The step was set as 5 μm for both horizontal and vertical directions. The peak spacing between E^1_{2g} and A_{1g} was increased from 21~23 to 25~27 cm^{-1} after sulfurization annealing, as shown in Fig. S5e and f. The corresponding Raman mapping images were shown in the insets. The morphology of 40% H_2 (annealed) sample was more uniform than that of 40% H_2 sample, indicating the improved crystal structure of the resultant MoS_2 film. The samples for 80% H_2 and 80% H_2 (annealed) had similar results, as shown in Fig. S5g and 5h. Furthermore, two prominent photoluminescence (PL) peaks at 627 and 677 nm were observed for the thus-synthesized films (Fig. 6j), suggesting that the annealing treatment with sulfur significantly improved the quality of MoS_x films and the high-crystallinity MoS_2 films with perfect S/Mo atomic ratio have be obtained.

Recently, P. K. Chow, *et al*. proposed a simple way to evaluate the defectiveness of 2D TMDCs nanosheets by thoroughly studying the evolution of PL and Raman spectra under exposure to intentionally created defects.[28] As for MoS_2 films, PL fitting B-exciton ($X^{O,B}$) and defect-related (X^D) peaks were closely related to defects. The samples at critical and representative H_2 content, including 5%, 10%, 20%, 40%, 80%, and 100%, were analyzed based on the working mechanism

illustrated in Fig. 5. The spectral weights of charged exciton (X^T), A-exciton ($X^{O,A}$) and $X^{O,B}$ were calculated and plotted in Fig. S6. The results can be explained according to Ref. [28]. The spectral weight of $X^{O,B}$ at 5% H_2 was lower than that at 10% H_2, due to the thermal-induced etching effect when H_2 content was relatively low. When H_2 content was set between 10% and 80%, the spectral weight of $X^{O,B}$ was nearly constant, in agreement with the previous speculation. That is, continuous MoS_2 films with high crystallinity and nearly perfect S/Mo atomic ratio could be obtained after sulfurization annealing in the range of 20%~80% H_2. When H_2 content was higher than 80%, the spectral weight of $X^{O,B}$ was decreased sharply and the defect-induced X^D peak emerged at 100% H_2, further confirming the irreversible circle-like vacancy defects generated during the first-step annealing at H_2 content exceeding 100% (As shown in Fig. 2i and k). No obvious change in Raman spectra was observed for these annealed samples, as shown in Fig. S6i. High resolution transmission electron microscopy (HRTEM) characterization was carried out for 40% H_2 samples before and after sulfurization annealing. Many sulfur-deficiency sites can be observed in Fig. 6k. After sulfurization annealing, the MoS_2 film with high crystalline structure and well-arranged atoms was obtained (Fig. 6l).

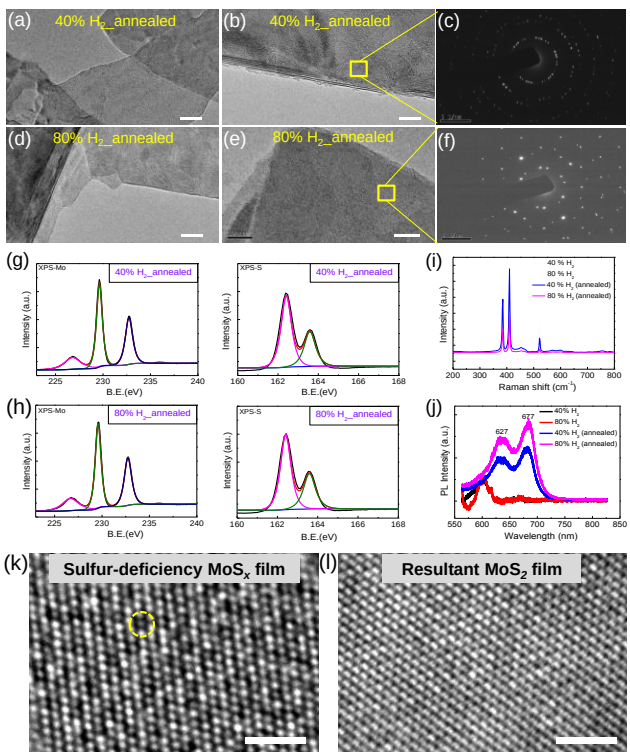

Figure 6. TEM characterizations of the samples after sulfurization annealing: (a,b) 40% H_2; (d,e) 80% H_2; (c,f) Corresponding SAED patterns of marked regions in (b,e). XPS spectra of Mo and S in MoS_2 films: (g) 40% H_2; (h) 80% H_2. (i) Raman and (j) PL spectra of the samples before and after sulfurization annealing. HRTEM images of 40% H_2 sample (k) before and (l) after sulfurization annealing. Scale bars: 50 nm in (a) and (d); 10 nm in (b) and (e); 2 nm in (k) and (l).

The results of TEM, XPS, Raman (mapping), and PL analysis unravelled the reproduction of Mo-S chemical bonding. The energetically active S atoms would be adsorbed on the remained unstable Mo sites during the high-temperature annealing in S atmosphere, breaking weak MoO_x structure and forming more stable S-Mo-S crystal structures. The schematic of the films before and after this process was demonstrated in Fig. S4a. The MoS_2 films could be successfully prepared by the sulfurization process, which, furthermore, could provide experimental evidences of the hydrogen-promoting desulfurization and oxidation reaction at high H_2 contents.

Table 1. XPS analysis for the samples after sulfurization annealing.

Samples	S2p (at.%)	Mo3d (at.%)	S/Mo
40% H_2	56.30	43.70	1.29
80% H_2	37.62	62.38	0.60
40% H_2 (annealed)	67.21	32.79	2.05
80% H_2 (annealed)	67.04	32.96	2.03

Circle-like defects in the samples were observed at high H_2 contents (>100%), as demonstrated in Fig. 2i-l. These defects may transform to more energy-stable states in shape size with increasing the H_2 content. This morphological damage may be originated from both the desulfurization and the oxidation etching effect at high concentration H_2 flow. Recently, a facile methodology to assemble metal particles on CVD-graphene films has been reported by employing the intrinsic wrinkles and defects of graphene.[29] Subsequent preparation of graphene nanopatches on graphene films provided a new approach of direct CVD mending, leading to p-type doping and electrical conductivity enhancement of graphene.[29] Similar to graphene films, MoS_2 films with defects may provide more active sites as well, which would be favour of metal particle loading. In recent years, 2D van der Waals heterostructures has been rapidly developed.[30] Due to the interfacial contamination issues in the process of layer-by-layer stacking, direct CVD fabrication of heterostructures seem to be more attractive in the near future. The preparation of 2D heterostructures through secondary CVD growth by using the defect-induced effect might have great application potential in 2D flexible nanoelectronics.

Conclusions

The roles of H_2 in CVD growth of MoS_2 films have been systematically studied by elaborately regulating the H_2 content in Ar atmosphere. Two roles of H_2 were found in the formation of the precursor MoS_x films by CVD: i) as an inhibitor of thermal-induced etching effect in the process of continuous films growth, and ii) as a promoter of desulfurization reaction by decreasing S/Mo atomic ratio and oxidation reaction of the obtained MoS_x films. High H_2 content of more than 100% in Ar would cause defect generation on the film and damage the continuity and uniformity of the film. Second-step sulfurization annealing was further conducted to understand the preparation

working mechanism of the film at high H_2 content. Continuous MoS_2 films with high crystallinity and nearly perfect S/Mo atom ratio were finally obtained after sulfurization annealing no matter what MoS_x films were formed at H_2 content in the range of 20%~80%. Thus the most challenging part would be how to evaluate the electrical performance of MoS_2 films prepared after annealing in Ar and S atmosphere. This work represents the first attempt of the working mechanism of H_2 on CVD formation of MoS_2 films. Moreover, tailoring MoS_2 films with different crystal structures by simply regulating the growth atmosphere would have a significant implication in fabricating 2D hybrid nanostructures and broaden the range of functional applications in microelectronics.

Acknowledgements

This work was supported by the National Science Foundation of China (51372133) and Tsinghua National Laboratory for Information Science and Technology (TNList) Cross-discipline Foundation.

Notes and references

[a]School of Materials Science and Engineering, State Key Laboratory of New Ceramics and Fine Processing, Tsinghua University, Beijing 100084, China. Email: hongweizhu@tsinghua.edu.cn.
[b]Center for Nano and Micro Mechanics, Tsinghua University, Beijing 100084, China.
[c]National Center for Nanoscience and Technology, Zhongguancun, Beijing 100190, China.
[d]Tsinghua National Laboratory for Information Science and Technology (TNList), Institute of Microelectronics, Tsinghua University, Beijing 100084, China.
Electronic Supplementary Information (ESI) available: Low-magnification optical images; Raman spectra of 0% and 5% H_2 samples; AFM characterizations; Schematic of the film before and after sulfurization annealing; Schematic illustrations of two typical Raman-active phonon modes (E^1_{2g}, A_{1g}); Raman (mapping) spectra for 40% and 80% H_2 samples before and after sulfurization annealing; PL spectra. See DOI: 10.1039/b000000x/

1. K. S. Novoselov, A. K. Geim, S. V. Morozov, D. Jiang, Y. Zhang, S. V. Dubonos, I. V. Grigorieva and A. A. Firsov, *Science*, 2004, **306**, 666.
2. M. J. Allen, V. C. Tung and R. B. Kaner, *Chem. Rev.*, 2010, **110**, 132.
3. C. Soldano, A. Mahmood and E. Dujardin, *Carbon*, 2010, **48**, 2127.
4. R. Ganatra and Q. Zhang, *ACS Nano*, 2014, **8**, 4074.
5. D. Jariwala, V. K. Sangwan, L. J. Lauhon, T. J. Marks and M. C. Hersam, *ACS Nano*, 2014, **8**, 1102.
6. A. Splendiani, L. Sun, Y. Zhang, T. Li, J. Kim, C. Y. Chim, G. Galli and F. Wang, *Nano Lett.*, 2010, **10**, 1271.
7. G. Eda, H. Yamaguchi, D. Voiry, T. Fujita, M. Chen and M. Chhowalla, *Nano Lett.*, 2011, **11**, 5111.
8. H. Li, J. Wu, Z. Yin and H. Zhang, *Acc. Chem. Res.*, 2014, **47**, 1067.
9. S. Bae, H. Kim, Y. Lee, X. Xu, J. S. Park, Y. Zheng, J. Balakrishnan, T. Lei, H. R. Kim, Y. I. Song, Y. J. Kim, K. S. Kim, B. Özyilmaz, J. H. Ahn, B. H. Hong and S. Iijima. *Nat. Nanotechnol.*, 2010, **5**, 574.
10. K. K. Kim, A. Hsu, X. Jia, S. M. Kim, Y. Shi, M. Dresselhaus, T. Palacios and J. Kong, *ACS Nano*, 2012, **6**, 8583.
11. Y. H. Lee, X. Q. Zhang, W. Zhang, M. T. Chang, C. T. Lin, K. D. Chang, Y. C. Yu, J. T. W. Wang, C. S. Chang, L. J. Li and T. W. Lin. *Adv. Mater.*, 2012, **24**, 2320.
12. K. K. Liu, W. Zhang, Y. H. Lee, Y. C. Lin, M. T. Chang, C. Y. Su, C. S. Chang, H. Li, Y. Shi, H. Zhang, C. S. Lai and L. J. Li. *Nano Lett.*, 2012, **12**, 1538.
13. Y. Zhan, Z. Liu, S. Najmaei, P. M. Ajayan and J. Lou, *Small*, 2012, **8**, 966.
14. Y. C. Lin, W. Zhang, J. K. Huang, K. K. Liu, Y. H. Lee, C. T. Liang, C. W. Chu and L. J. Li, *Nanoscale*, 2012, **4**, 6637.
15. S. Wu, C. Huang, G. Aivazian, J. S. Ross, D. H. Cobden and X. Xu, *ACS Nano*, 2013, **7**, 2768.
16. I. Vlassiouk, M. Regmi, P. Fulvio, S. Dai, P. Datskos, G. Eres and S. Smirnov, *ACS Nano*, 2011, **5**, 6069.
17. M. Losurdo, M. M. Giangregorio, P. Capezzuto and G. Bruno, *Phys. Chem. Chem. Phys.*, 2011, **13**, 20836.
18. X. Zhang, J. Ning, X. Li, B. Wang, L. Hao, M. Liang, M. Jin and L. Zhi, *Nanoscale*, 2013, **5**, 8363.
19. B. Wu, D. Geng, Z. Xu, Y. Guo, L. Huang, Y. Xue, J. Chen, G. Yu and Y. Liu, *NPG Asia Materials*, 2013, **5**, e36.
20. R. K. Sahoo, H. Mamgain and C. Jacob, *Bull. Mater. Sci.*, 2014, **37**, 1197.
21. Y. Zhang, Y. Zhang, Q. Ji, J. Ju, H. Yuan, J. Shi, T. Gao, D. Ma, M. Liu, Y. Chen, X. Song, H. Y. Hwang, Y. Cui and Z. Liu, *ACS Nano*, 2013, **7**, 8963.
22. C. Lee, H. Yan, L. E. Brus, T. F. Heinz, J. Hone and S. Ryu, *ACS Nano*, 2010, **4**, 2695.
23. J. Wu, H. Li, Z. Yin, H. Li, J. Liu, X. Cao, Q. Zhang and H. Zhang, *Small*, 2013, **9**, 3314.
24. X. Lu, M. I. B. Utama, J. Zhang, Y. Zhao and Q. Xiong, *Nanoscale*, 2013, **5**, 8904.
25. Y. K. Huang, J. D. Cain, L. Peng, S. Hao, T. Chasapis, M. G. Kanatzidis, C. Wolverton, M. Grayson and V. P. Dravid, *ACS Nano*, 2014, **8**, 10851.
26. W. Park, J. Baik, T. Y. Kim, K. Cho, W. K. Hong, H. J. Shin and T. Lee, *ACS Nano*, 2014, **8**, 4961.
27. J. L. Brito, M. Ilija and P. Hernfindez, *Thermochimica Acta*, 1995, **256**, 325.
28. P. K. Chow, R. B. Jacobs-Gedrim, J. Gao, T. M. Lu, B. Yu, H. Terrones and N. Koratkar, *ACS Nano*, 2015, **9**, 1520.
29. W. Song, K. W. Kim, S. J. Chang, T. J. Park, S. H. Kim, M. W. Jung, G. Lee, S. Myung, J. Lim, S. S. Lee and K. S. An, *J. Mater. Chem. C*, 2015, **3**, 725.
30. A. K. Geim and I. V. Grigorieva, *Nature*, 2013, **499**, 419.

